# Momentum imaging of dissociative electron attachment to N_{2}O at the 2.3-eV shape resonance

A. Moradmand, A. L. Landers, and M. Fogle

Phys. Rev. A **88**, 012713 — Published 24 July 2013

DOI: 10.1103/PhysRevA.88.012713

# Momentum imaging of dissociative electron attachment to $N_2O$ at the 2.3 eV shape resonance

A. Moradmand, A. L. Landers, and M. Fogle*
*Department of Physics, Auburn University, Auburn, AL 36849*
(Dated: July 9, 2013)

We report ion momentum imaging measurements of dissociative electron attachment to $N_2O$ near the well-known 2.3 eV shape resonance. We have made a comparison to previous results and have used the formalism of O'Malley & Taylor[1] to calculate angular $O^-$ anion fragment distributions. Using these angular distributions along with the axial recoil approximation, we show a predominant $\Pi$ contribution to the observed angular $O^-$ distribution with no significant indication of a $\Sigma$ contribution, as previously reported. We conclude that the dissociation takes place in a near-linear geometry and proceeds across a Renner-Teller barrier.

PACS numbers: 34.80.Ht

## I. INTRODUCTION

The dissociative electron attachment (DEA) reaction to nitrous oxide

$$e^- + N_2O \rightarrow N_2O^{-*} \rightarrow N_2(^1\Sigma_g) + O^-(^2P)\ , \quad (1)$$

which produces $O^-$ anion fragments, has been studied by various experimental and theoretical researchers [3–11]. Nitrous oxide has a linear equilibrium geometry represented by a $C_{\infty v}$ point group. Upon bending the symmetry is lowered to $C_{1h}$. The structure of the $N_2O^-$ negative ion has been summarized by Bardsley [2]. Two predominant resonances have been identified in DEA to $N_2O$ at 0.7 eV and 2.3 eV [2, 4, 6]. The lowest energy resonance has been assigned to a $^2\Sigma$ state that is highly temperature dependent [4, 9]. The 2.3 eV resonance has been attributed to a mixture of $\Sigma$ and $\Pi$ states. There has been a considerable amount debate in the literature regarding the assignment of states to these resonances, particularly for the 2.3 eV resonance. The first angle-resolved DEA measurement was made by Tronc [5] over a range of 30–130°. The conclusion drawn from that work was that both a $\Pi$ and $\Sigma$ component were necessary to describe the measured $O^-$ angular fragment distribution. The joint theoretical and experimental work reported by Hopper et al. [6] suggested that the broad resonance at 2.3 eV was comprised of two close-lying resonances at 1.8 and 2.2 eV that could be assigned to $^2\Sigma$ and $^2\Pi$ states, respectively. They also noted that excitation of the symmetric stretch vibration would greatly facilitate the DEA reaction. The angle-dependent inelastic electron scattering experiments of Andric & Hall [7] seemed to confirm the two resonances predicted by Hopper et al. suggesting that below 1.8 eV the $^2\Sigma$ state was dominant while above 2.4 eV the contribution was almost entirely from the $^2\Pi$ state. Vibrational excitation measurements by Allan & Skalický [10] assumed the 2.3 eV was attached to a $\pi^*$ state that splits into $A'$ and $A''$ upon bending. They found no evidence of a $\sigma^*$ state in the 1.5–2.5 eV energy range, although they noted that the $A'$ branch of the $\pi^*$ resonance could be considered as $\sigma^*$ in chemical terms. It remains that the states involved near the 2.3 eV DEA resonance and their assigned character are unclear.

Recently, Xia et al.[11] have investigated the $O^-$ angular fragment distribution due to DEA over the energy range of 0.7–2.5 eV using an ion velocity imaging apparatus. Their apparatus, like the one also discussed in this work, allows for a more complete angular distribution measurement as compared to the early angular measurements by Tronc. The measurements reported by Xia et al. indicate a considerable $\Sigma$ contribution near the 2.3 eV resonance, which as we will discuss, predicts a considerable amount of bending dynamics driven by attachment. Upon bending, the degenerate $^2\Pi$ state splits into $^2A'$ and $^2A$". Given that the identification of this bending dynamic is key to assigning the character of the resonance to $\Sigma$ and/or $\Pi$, we will treat the molecule in the lower bent symmetry. It is the focus here to investigate the dynamics driven by DEA via the $\Sigma$ and $\Pi$ contributions to the 2.3 eV resonance by applying an ion momentum imaging technique that utilizes a cold target formed by a supersonic expansion gas jet. The measured $O^-$ angular fragment distribution will then be compared to previous work.

## II. EXPERIMENT

The apparatus used for this study has been described in detail elsewhere [12], however a brief overview will be given. Figure 1 shows a schematic of the momentum imaging apparatus at Auburn University. To form a molecular target, medical-grade nitrous oxide was adiabatically expanded through a 10 $\mu$m nozzle to form a supersonic gas jet. A 300$\mu$m skimmer then selected the central portion of this jet to form a molecular beam that was passed into the interaction region. A residual gas analyzer was used to verify that the primary gas load to the interaction region was nitrous oxide. A liquid nitro-

*fogle@physics.auburn.edu

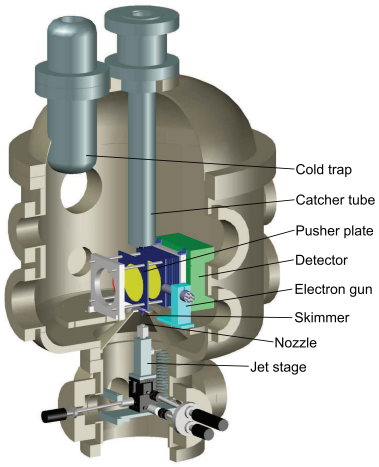


FIG. 1: Schematic of the momentum imaging apparatus.

gen cold trap was used to reduce the partial pressures of other residual gas components in the interaction region.

The molecular beam was crossed orthogonally in an electrostatically field-free region by a 100 ns, 40 kHz pulsed electron beam of $2.3 \pm 0.3$ eV. After each electron pulse, a pusher plate was pulsed from ground to -30 V after an 800-ns delay. This resulted in complete $4\pi$ collection of $O^-$ anion fragments that were then directed towards an 80-mm microchannel plate with a delay-line anode for position determination. The time-of-flight is also recorded between the electron pulse and the particle impact on the detector. The position and timing information allow for a complete determination of the initial momentum vector of the anion fragment upon dissociation. Recorded dissociation event data are then analyzed off line by defining a dissociation sphere through which slicing planes can be defined to observe angular fragment distributions. As can be seen in Fig. 2, such a momentum sphere slice is presented to show the $O^-$ fragment distributions in momentum space. It is important to note that such a slice of the momentum sphere needs to be appropriately weighted for solid angle, otherwise particles with low kinetic energy release would be over-emphasized. This is accomplished in our analysis by defining a wedge selection gate (see top pane of Fig. 2) that is then integrated around the slicing plane of the momentum sphere.

From the data shown in Fig. 2, both kinetic energy release and angular distributions of $O^-$ fragments can be generated. Figure 3 shows the kinetic energy release distribution of $O^-$ fragments as compared to the previous results of Chantry [4] and Xia et al. [11]. Our current results are in good agreement with these previous measurements. We note that the peak of the kinetic energy distribution from Xia et al. is approximately 0.1 eV below our current data. We have excellent agreement with the kinetic energy distribution of Chantry, with the exception of the low-energy region below 0.2 eV. We note that our kinetic energy distribution exhibits a small shoulder contribution between 0.1–0.2 eV which could be attributed to another channel resulting in excited fragments.

Figure 4 shows the angular distribution of $O^-$ fragments and makes a comparison to the fitted results of Xia et al. [11]. We will make an extended comparison of these angular distributions in what follows.

## III. RESULTS AND DISCUSSION

If we describe the $N_2O$ molecule in Jacobi coordinates, assuming that the N–N bond length remains unchanged during the attachment and dissociation process and that the O atom can be described by an angle and distance from the center of the N–N bond, we can treat the system as a quasi-diatomic and use the formalism of O'Malley and Taylor[1] to describe the the angle-dependent DEA cross section as

$$\sigma_{DA}(\theta) \propto \left|a_0 Y_{00} + e^{i\delta_1} a_1 Y_{10} + e^{i\delta_2} a_2 Y_{20}\right|^2 + \left|b_0 Y_{11} + e^{i\delta_3} b_1 Y_{21} + e^{i\delta_4} b_2 Y_{31}\right|^2 \quad (2)$$

where $Y_{\mu l}$ are the spherical harmonics of the partial waves of the incident electrons of angular momentum, $l$. $|\mu| = |\Lambda_f - \Lambda_i|$ is the difference in the projection of the angular momentum on the internuclear axis, $a_i$ and $b_i$ are weighting constants and $\delta_i$ is a parameter that accounts for the phase lag induced by the interaction potential. We have constructed the total relative cross section from two terms with the first term representing a $\Sigma$ contribution and the second term representing a $\Pi$ contribution. Only the first few partial waves are included in each term as it is expected that higher partial waves will not contribute given the low electron energy. These two terms can be treated individually and we will describe how the individual contributions represent our measured angular $O^-$ fragment distribution as well as compare to a similar fit performed by Xia et al. to their observed angular distribution.

We should point out that the connection between the measured angular distribution of fragments and the angle-dependence of the DEA cross section can only be related in a straight-forward manner if the axial recoil approximation holds. This is true for $N_2O$ if dissociation

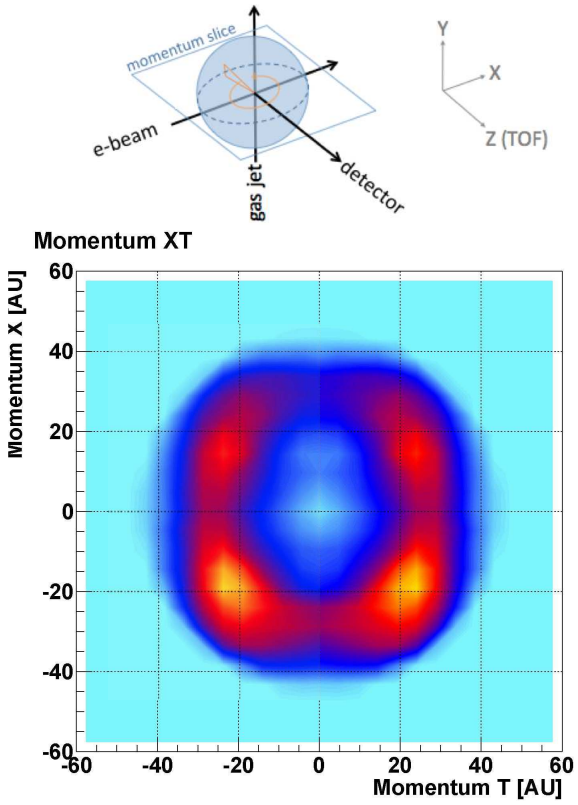


FIG. 2: (top) a schematic of the dissociating momentum sphere and the associated coordinate system adopted for analysis. See the text for more details regarding momentum slicing and weighting. (bottom) The momentum-space distribution of $O^-$ anion fragments, at 2.3 eV electron attachment energy, in the plane defined by the electron beam and time-of-flight axes of the coordinate system.

occurs via a linear geometry and if the dissociation of the TNI is fast compared to its rotation in the laboratory frame. The $\Sigma$ component discussed above is a result of significant bending upon attachment where the axial recoil approximation breaks down. This manifests in the observed angular distribution of $O^-$ fragments as having $\Sigma$ character and is not necessarily indicative of a $\Sigma$ attachment state directly. Additional theoretical guidance will be necessary to investigate the details of any bending dynamics that occurs in the DEA of $N_2O$.

Figure 4(a) shows the $O^-$ angular fragment distribution results of Xia et al.[11] for an incident electron energy of 2.25 eV along with the $\Sigma$ and $\Pi$ contributions obtained from their fit coefficients. Figure 4(b) shows our measured $O^-$ angular fragment distribution for an incident electron energy of 2.3 eV. The two experiments obtain significantly different angular distributions with the data of Xia et al. showing a more pronounced forward-backward asymmetry while our results show a more pronounced tetra-petal lobed distribution.

Xia et al. use the same partial wave formalism as shown by Eqn. 2 to systematically fit their results and

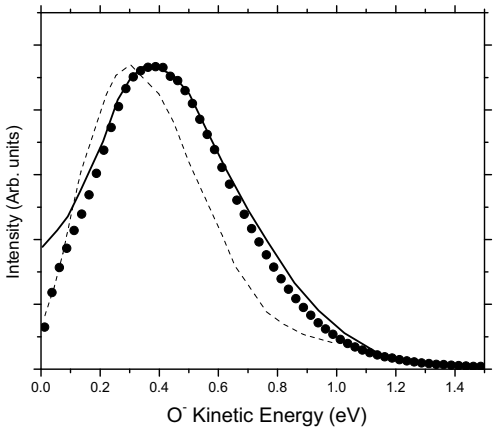


FIG. 3: Kinetic energy release distribution of $O^-$ fragments. Current results - filled circles, Chantry [4] - solid curve, Xia et al. [11] - dashed curve. All data sets are normalized to the same arbitrary peak intensity.

arrive at fitting values of $a_0 = 1.00$, $a_1 = 0.57$, $a_2 = 0.29$, $b_0 = 0.75$, $b_1 = 0.72$, $b_2 = 0.45$, $\delta_1 = 2.601$ rad, $\delta_2 = 1.312$ rad, $\delta_3 = 2.096$ rad and $\delta_4 = 0.716$ rad. The thin solid curves in Fig. 4(a) indicate the $\Sigma$ and $\Pi$ terms from their fit coefficients. We note that we were unable to reproduce their exact same fit to their data using the fitting coefficients provided. What is important, however, is the relative contributions of the $\Sigma$ and $\Pi$ components. We also found no indication that the experimental angular resolution was incorporated into the fit of angular fragment data. As we intend to show, this can lead to exaggerated contributions of the fitting terms and ultimately misguide the interpretation of the data.

The angular resolution is limited by the uncertainty in the initial electron interaction direction and can be approximated by the transverse and parallel electron velocities, with respect to the axis of the uniform magnetic guiding field, as

$$\Delta\theta \simeq \tan^{-1}\left(\frac{E_\perp}{E_\parallel}\right)^{1/2}, \qquad (3)$$

which results in an angular resolution of approximately 20° (FWHM). We expect the angular resolutions of the experiment of Xia et al. and our apparatus to be similar based on the electron sources.

In determining the contributions of the $\Sigma$ and $\Pi$ terms of Eqn. 2 to the observed angular data, we should keep in mind that we are attempting to gauge the bending dynamic of dissociation. If dissociation occurs in a linear configuration under the axial recoil approximation, then we would expect the distribution to be explained solely by a $\Pi$ contribution. If the bending cannot be solely explained by a $\Pi$ contribution then a $\Sigma$ component must be added. The amount of this $\Sigma$ component is connected

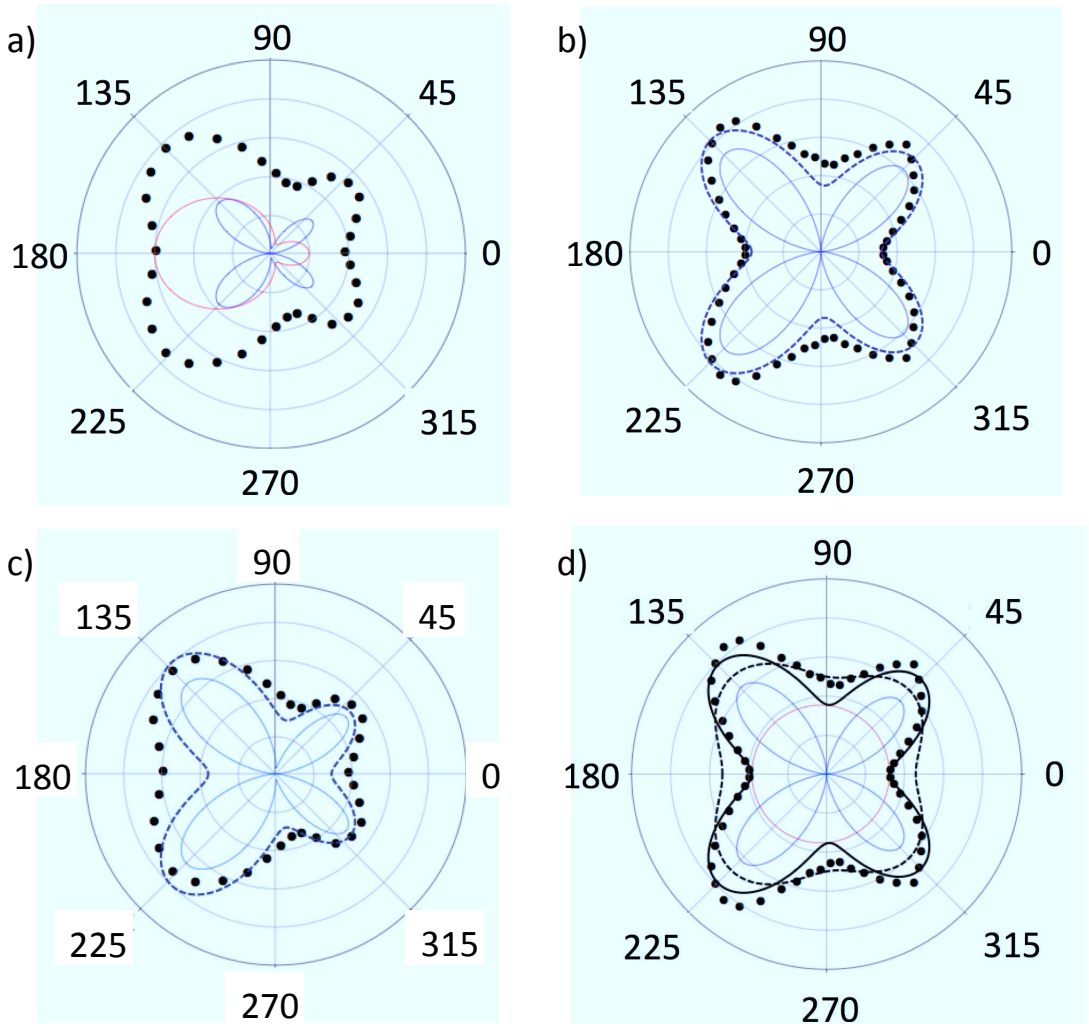


FIG. 4: (a) The $O^-$ angular fragment distribution experimental results of Xia et al.[11] measured for 2.25 eV electrons. The inner thin lines represent the $\Sigma$ (forward-backward lobed) and $\Pi$ (tetra-petal lobed) contributions from their fit coefficients using Eqn. 2. (b) Our experimental $O^-$ angular fragment distribution for 2.3 eV electrons. The inner thin curve represents a $\Pi$ contribution. The dashed curve is the $\Pi$ contribution convoluted with the experimental angular resolution. See the text for more details regarding the determination of angular resolution and the determination of the $\Pi$ contribution. (c) The thin curve is a representation from Eqn. 2 of the data of Xia et al. using just a $\Pi$ contribution. The dashed curve is the convolution of that $\Pi$ contribution by the expected experimental angular resolution. (d) An example (see text for details) of how fitting directly with Eq. 2 without the consideration of angular resolution can lead to an exaggerated $\Sigma$ contribution. The thin inner curves are the $\Sigma$ and $\Pi$ contributions. The thick solid curve is the sum of these contributions. The dashed curve is the summed contribution convolved with the expected experimental angular resolution.

to the degree of bending in the dissociation process. We would not expect a pure $\Sigma$ component to explain the angular distribution. For completeness sake, we have attempted to describe our angular distribution solely with the $\Sigma$ term of Eqn. 2, however, no combination of constants and phase lags can describe the intense tetra-petal lobes we observe. On the other hand, we have attempted to describe our observed $O^-$ distribution solely with the $\Pi$ term and this results in a more reasonable representation of our results if the angular resolution of the experimented is also considered. We don't expect the phase lags to be appreciably different in comparing data sets so we have fixed these at the values reported by Xia et al. We have then adjusted the relative contributions of the $p\Pi$, $d\Pi$ and $f\Pi$ partial waves to best reflect our observed distribution by making changes to the $b_i$ constants. It is not our intention to make a rigorous fit but to qualitatively show how the various contributions of the $\Pi$ term can be used to describe the observed $O^-$ distribution. We have used the peaks of the tetra-petal lobes in our observed angular distribution to gauge the weighting constants. We note that no $f\Pi$ contribution is neces-

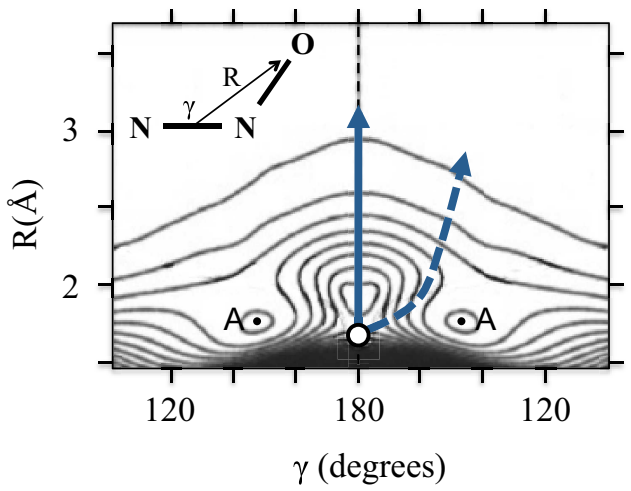


FIG. 5: The $^2$A' potential energy surface of $N_2O^-$ reproduced from Suter & Greber [13]. The Jacobi coordinate system used is shown in the upper left inset. The thick solid curve illustrates direct dissociation along a linear geometry. The thick dashed curve illustrates dissociation along a bending geometry. The points labeled *A* represent the $N_2O^-$ equilibrium geometry. The open circle represents the vertical Franck-Condon transition from the neutral molecule state.

sary, which is not unreasonable given the low electron energy. This is gauged by the angle between the tetrapetal lobes and the incident electron direction. We note that the forward-backward asymmetry, with respect to the incoming electron, is governed primarily by the contribution of the $p\Pi$ component. We have selected the $b_0$ constant so as to have forward-backward relative peak intensities comparable to our measurement. Our final weighting constant values are $b_0 = 0.1$, $b_1 = 0.8$ and $b_2 = 0.0$. This results in the thin solid curve shown at the center of Fig. 4(b). We then convolute the calculated angular dependence by 20° (FWHM) to account for the angular resolution of the experiment. This is represented by the dashed curve in Fig. 4(b). We note that once the angular resolution is incorporated, no significant $\Sigma$ contribution is then needed to effectively explain the observed $O^-$ angular distribution. We do, however, note that there is some additional contribution at orthogonal angles that isn't accounted for.

Given the number of fit coefficients, there is no guarantee of uniqueness to a fit, i.e., it might be possible that another combination of $\Sigma$ and $\Pi$ partial waves results in a similar fit representation. It is not straightforward to test the global fitting parameter space while including the effects of angular resolution, however, as can be seen in Fig. 4(b), the inclusion of the angular resolution does support a much stronger relative $\Pi$ contribution as compared to the significant $\Sigma$ contributions reported previously.

The adverse effects of fitting without the consideration of angular resolution are demonstrated by an example shown in Figure 4(d). We have taken our $\Pi$ component from Eqn. 2, as discussed above, and have added a $\Sigma$ component (fit coefficients: $a_0 = 1.05$, $a_1 = 0.03$ and $a_2 = 0.00$) in an attempt to represent our angular distribution data. The sum of these components yields the solid curve in Fig. 4(d). This sum represents the experimental angular distribution data to a similar degree of fit as shown by the dashed curve in Fig. 4(b) and suggests that the $\Sigma$ contribution is comparable in magnitude to the $\Pi$ contribution, as reported previously. The summed contribution in Fig. 4(d), however, does not account for the angular resolution of the experiment. If the angular resolution is then considered, the dashed curve in Fig. 4(d) results, which does not represent the data well. The conclusion of this example is that fitting directly with Eqn. 2 without consideration of experimental angular resolution can yield an exaggerated $\Sigma$ contribution. To further show the importance of considering the angular resolution, we have attempted to represent the data of Xia et al. with just a $\Pi$ contribution as shown in Fig. 4(c). The inner thin curve shows the resulting $\Pi$ contribution, although with different partial wave weighting constants as compared to Fig. 4(b) (fitting coefficients: $b_0 = 0.5$, $b_1 = 0.6$ and $b_2 = 0.3$). The dashed curve shows the $\Pi$ contribution convoluted by the expected angular resolution. As can be seen, this representation suggests

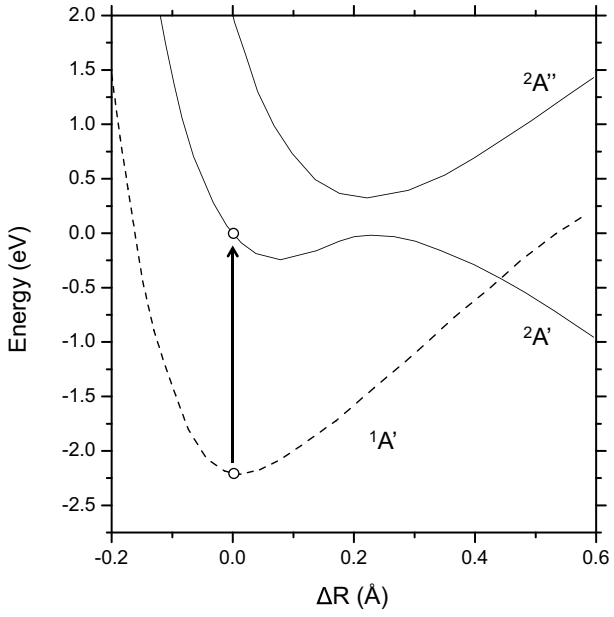


FIG. 6: The potential energy curves of Suter & Greber [13] along $\gamma = 180°$ (see Fig. 5). The $^1$A' curve represents the neutral $N_2O$. The $N_2O^-$ $^2$A' curve leads to direct dissociation while the $N_2O^-$ $^2$A" curve forms an avoided crossing with $^2$A'. The vertical arrow indicates the Franck-Condon transition upon electron attachment.

that a considerable amount of Π contribution can partially represent their data well if the angular resolution is considered. There is an indication that some amount of Σ may be necessary to account for the forward-backward portion of the angular distribution although the relative contribution of the Π term is considerably more than determined by a direct fit using Eqn. 2.

In deciphering the meaning attached to these different state contributions, it is necessary to have an idea of the potential energy landscape on which the attachment and dissociation take place. In Fig. 5 we have reproduced the $^2A'$ potential energy surface calculated by Suter & Greber[13]. As these authors note, a Renner-Teller "reef" is present along the linear configuration as the $R$ coordinate increases. A slice of the $^2A'$ potential energy surface along $\gamma = 180°$ is shown in Fig. 6 along with the $^2A''$ and neutral $N_2O$ ($^1A'$) potential energy curves. In Fig. 5, two potential dissociation paths of $N_2O^-$ are shown. The path represented by the solid curve is a direct dissociation resulting from a linear (or near linear) geometry. The path represented by the dashed curve is associated to a predominant bending dynamic that takes place as the TNI approaches the equilibrium $N_2O^-$ geometry during dissociation. The dissociation path that goes directly out over the Renner-Teller "reef" is along the $^2A'$ ($^2\Pi$) state and is associated to the Π contribution term of Eqn. 2. The dissociation path that proceeds via a bending dynamic is also on the $^2A'$ surface but is in the bending coordinate that lifts the degeneracy of the $^2\Pi$ state. The bending dissociation path thus has a Σ character, as pointed out by Allan & Skalický [10]. If bending is present in the dissociation, we would expect some addition of Σ to the Π angular distribution. As we pointed out earlier, the degree to which a Σ component is added is directly related to the amount of bending.

Andric & Hall [7] suggested that the relative $O^-$ formation cross section ratio associated to the Π and Σ states is approximately 2:1 at the 2.3 eV resonance. Likewise, Xia et al. show that the Σ contribution falls off rapidly as the electron energy increases towards the DEA resonance peak near 2.3 eV. They report a relative contribution ratio of approximately 1:1. Our results suggest that if the angular resolution is considered in the use of Eqn. 2, the Π contribution is predominant at 2.3 eV. We would further point out that our attempt to represent the data of Xia et al. by just a Π contribution, with angular resolution incorporated, also suggests that the previously determined relative contribution of a Σ component is likely overestimated. It is unclear as to the effective differences in the various experiments that could lead to these disparate results but it could be an indication of different experimental parameters, e.g., interaction volume overlap size or gas target temperature. As has been pointed out in previous work, the 0.7 eV resonance is strongly temperature dependent and is Σ in character. Xia et al. seem to show a considerable contribution at the 0.7 eV interaction energy which could be an indication of their target temperature. The measured temperature dependence of this resonance shows that it is dramatically reduced below approximately 300K [4, 9]. It is unclear if a high-energy tail portion of the 0.7 eV resonance, as shown by Chantry, could be contributing partially to the the observed contribution at the 2.3 eV resonance. Our current apparatus uses a supersonic gas jet to form the target at a temperature of approximately 15K. Our gas jet also forms a well localized target less than 2 mm wide at the interaction. It would be particularly interesting to investigate the $N_2$ dissociation fragments as the bending dynamic associated to the Σ contribution would lead to considerable rotational excitation while the direct dissociation along the Renner-Teller reef would lead to vibrational excitation. Regardless, this particular interaction has seen significant progress, however, more refined theoretical tools and additional experiments are likely to be needed to further interpret the experimental results obtained so far.

## IV. CONCLUSION

We have investigated the dissociative electron attachment of $N_2O$ near the well-known 2.3 eV resonance using an ion momentum imaging apparatus. The measurements resulted in detailed kinetic energy and $O^-$ angular fragment distributions that were then compared to previous results and calculated angular distributions based on the formalism of O'Malley & Taylor [1]. We find that the incorporation of experimental angular resolution is crucial in determining partial wave contributions.

Our measured angular distributions of $O^-$ suggest that the dominant interaction state at 2.3 eV is $^2\Pi$. This is in contradiction to the recent ion velocity imaging results of Xia et al. [11] that indicate a considerable Σ contribution along with a Π component and that this is indicative of a bending dynamic that occurs upon attachment. Our observation of a predominant Π contribution, with little to no Σ component suggests that the dissociation is via the linear (or near linear) configuration and proceeds across a Renner-Teller barrier.

[1] T. O'Malley and H. Taylor, Phys. Rev. **176**, 207 (1968).
[2] J. Bardsley, J. Chem. Phys. **51**, 3384 (1969).
[3] G. Schultz, J. Chem. Phys. **34**, 1778 (1961).
[4] P. Chantry, J. Chem. Phys. **51**, 3369 (1969).
[5] M. Tronc, F. Fiquet-Fayard, C. Schermanns, and R. I. Hall, J. Phys. B.: Atom. Molec. Phys. **10**, L459 (1977).
[6] D. Hopper, A. Wahl, R. Wu, and T. Tiernan, J. Chem. Phys. **65**, 5474 (1976).
[7] L. Andric and R. Hall, J. Phys. B.: At. Mol. Opt. Phys. **17**, 2713 (1984).
[8] E. Krishnakumar and S. Srivastava, Phys. Rev. A **41**, 2445 (1990).
[9] F. Bruning, S. Matejcik, E. Illenberger, Y. Chu, G. Senn, D. Muigg, G. Denifl, and T. Mark, Chem. Phys. Lett. **292**, 177 (1998).
[10] M. Alan and T. Skalicky, J. Phys. B.: At. Mol. Opt. Phys. **36**, 3397 (2003).
[11] L. Xia, B. Wu, H.-K. Li, X.-J. Zeng, and S. Tian, J. Chem. Phys. **137**, 151102 (2012).
[12] A. Moradmand, J. Williams, A. Landers, and M. Fogle, Rev. Sci. Instrum. **84**, 033104 (2013).
[13] H. Suter and T. Greber, J. Phys. Chem. B **108**, 14511 (2004).

## Acknowledgments

A.L.L would like to acknowledge support by DOE contract DE-FG02-10ER16146. The authors would like to thank Dan Slaughter for manuscript comments and discussion.